Compton scattering studies of the valence electron density distribution in GaAs

1990 J. Phys.: Condens. Matter 2 10517

(http://iopscience.iop.org/0953-8984/2/51/023)

J. Phys.: Condens. Matter 2 (1990) 10517–10528. Printed in the UK

Compton scattering studies of the valence electron density distribution in GaAs

D N Timms† ††, M J Cooper†, R S Holt‡, F Itoh§, T Kobayasi|| and H Nara¶

† Department of Physics, University of Warwick, Coventry CV4 7AL, UK
‡ Neutron Science Division, Rutherford Appleton Laboratory, Chilton, Didcot, Oxon OX11 0QX, UK
§ Department of Electronic Engineering, Faculty of Engineering, Gunma University, 1-5-1 Tenjin-Cho, Kiryu 376 Gunma, Japan
|| College of Medical Sciences, Tohoku University, Seiryo, Sendai 980, Japan
¶ Education Centre for Information Processing, Tohoku University, Kawauchi, Sendai 980, Japan

Received 28 June 1990

Abstract. Directional Compton profiles have been measured along the [100], [110], [111], [112] and [221] crystallographic axes in GaAs using 412 keV and 59.54 keV γ-radiation from ^{198}Au and ^{241}Am radioisotope sources, respectively. The results have been compared with the prediction of a pseudopotential calculation both in momentum space and in position space. The pseudopotential approach predicts the anisotropy of the valence electron distribution and is consistent with an increase in the ionic bond character compared with Ge. On the other hand, the total electron distributions are not well described due to the omission of core orthogonalisation terms.

1. Introduction

In recent years Compton scattering has proved to be a sensitive technique for investigating the electronic structure of solids [1,2]. The quantity observed experimentally is the Compton profile, $J(p_z)$ which is the projection of the one electron momentum density distribution, $n(\boldsymbol{p})$ along a line, p_z chosen to be parallel to the experimental scattering vector, $\boldsymbol{K}$ i.e.

$$J(p_z) = \int_{p_x} \int_{p_y} n(\boldsymbol{p})\, \mathrm{d}p_x\, \mathrm{d}p_y. \tag{1}$$

In tetrahedrally bonded semiconductors such as GaAs, the bonding is often described as being basically covalent with a degree of ionicity. In a purely covalent solid the anisotropy in $n(\boldsymbol{p})$ and hence in $J(p_z)$ is related to the degree of localisation of the bonding electrons, whereas for an ionic solid $n(\boldsymbol{p})$ is approximately isotropic. The anisotropy in $J(p_z)$, which is isolated by forming directional difference profiles, i.e.

$$\Delta J(p) = J_{h,k,l}(p) - J_{h',k',l'}(p) \tag{2}$$

†† Present address: Department of Applied Physics and Physical Electronics, Portsmouth Polytechnic, Park Building, King Henry I Street, Portsmouth PO1 2DZ, UK.

0953-8984/90/5110517+12$03.50

can provide information about both the bonding and also the degree of ionicity of the solid. Furthermore, this difference has the practical advantages of removing the isotropic core-electron contribution and eliminating many of the troublesome systematic errors in $J(p_z)$.

In a metal it is appropriate to consider the behaviour of the delocalised conduction electron gas in terms of its position space behaviour [3], Fermi surface, etc. The effect of electron correlation is to promote electrons from states within to momentum states outside the Fermi sphere and in Compton profile measurements the effect manifests itself as a broadening of $J(p_z)$ [4]. In localised systems such as semiconductors [5] it can be more informative to analyse Compton scattering data in position space by introducing the function $B(\boldsymbol{r})$, which is the autocorrelation function of the position space wavefunction

$$B(\boldsymbol{r}) = \int \psi(\boldsymbol{r}+\boldsymbol{r}')\psi(\boldsymbol{r}')\mathrm{d}\boldsymbol{r}'. \tag{3}$$

The projections of $B(\boldsymbol{r})$ are related to the Compton profile by a Fourier Transform [6]

$$B(z) = \int \psi^*(\boldsymbol{r}+\boldsymbol{z})\psi(\boldsymbol{r})\,\mathrm{d}\boldsymbol{r} = \int J(p_z)\exp(-\mathrm{i}p_z z)\,\mathrm{d}p_z. \tag{4}$$

This representation has several practical advantages. Firstly, it is conceptually simpler to interpret experimental results in position space rather than momentum space. Secondly, the deconvolution of the experimental data becomes a multiplicative process. Finally, the isotropic core-electron contribution and most residual systematic errors which are all slowly varying functions of momentum are restricted to a small region around the origin of $B(\boldsymbol{r})$, whereas the valence electron contribution extends further and these errors are therefore separable in $B(\boldsymbol{r})$.

For a crystalline solid the overlap integral, equation (3), may be written in terms of Bloch functions for the band electrons. Summing over all k states in each occupied band gives,

$$B(\boldsymbol{r}) = \sum_{k,\mu} n_\mu(\boldsymbol{k}) \int \psi_k^*(\boldsymbol{r}+\boldsymbol{r}')\psi_k(\boldsymbol{r}')\,\mathrm{d}\boldsymbol{r}' \tag{5}$$

where $n_\mu(\boldsymbol{k})$ is the occupation number of the kth state in the μth band. Expanding equation (5) in terms of one electron Bloch functions and evaluating $B(\boldsymbol{r})$ for any real lattice translation vector $\boldsymbol{r} = \boldsymbol{R}_\mathrm{L}$ gives [6],

$$B(\boldsymbol{R}_\mathrm{L}) = \frac{2}{V_\mathrm{BZ}} \int_\mathrm{BZ} n_\mu(\boldsymbol{k})\exp(-\mathrm{i}\boldsymbol{k}\cdot\boldsymbol{R}_\mathrm{L})\,\mathrm{d}\boldsymbol{k} \tag{6}$$

where V_BZ is the volume of the Brillouin zone. In insulators all bands are filled and $n(\boldsymbol{k})$=constant, therefore $B(\boldsymbol{r}) = 0$ for all $\boldsymbol{r} = \boldsymbol{R}_\mathrm{L}$ and hence the B-function of an insulator will cross the real space axis at all points corresponding to lattice translations. The measured zero-crossing points of $B(\boldsymbol{r})$ will be unaffected by the resolution damping and their correct location is a valuable check on the data processing procedure. For theoretical models the location of the lattice zeros confirms that the summation over k-states in all occupied bands has been performed correctly (see equation (5)). In metals the quantities $B(\boldsymbol{R}_\mathrm{L})$ are the Fourier components of the

occupation function $n_\mu(\boldsymbol{k})$. This is equivalent to the Lock–Crisp–West [8] theorem encountered in positron annihilation studies, where that method's superior resolution compared with Compton studies allows Fermi surfaces to be reconstructed [9]. The behaviour of the B-function between lattice zeros, namely its size and sign, may under certain circumstances provide information about the type of bonding between different elements in an atomic chain [7].

In an earlier Compton scattering study [10], five directional Compton profiles of the pure covalent semiconductors diamond, Si and Ge were measured with 160 keV γ-radiation. As these semiconductors all have the diamond structure but exhibit quite different electronic properties it was possible to determine whether or not the anisotropy in the Compton profile simply scaled with the lattice structure: in fact the anisotropy in $J(p_z)$ is not determined solely by the lattice structure. These results prompted a profusion of theoretical calculations of $J(p_z)$ for these materials for example, Hartree–Fock [11], LCAO [12] and pseudopotential [13] calculations.

Highly accurate Compton profiles of Ge and Si have also been measured along the [110] crystallographic direction by Pattison and Schneider [5] and in this case the data interpreted using the long range autocorrelation of the electronic wavefunctions obtained directly from $B(z)$ (equation (4)): the B-function of Si was found to be in excellent quantitative agreement with a LCAO calculation [12].

Individual Compton profiles are projections of the total momentum distributions, $n(\boldsymbol{p})$ (see equation (1)). A method for reconstructing $n(\boldsymbol{p})$ from a series of directional Compton profiles has been developed [14] and used to reconstruct the electron momentum density of Si from six directional profiles measured with 412 keV ^{198}Au γ-radiation. The results were found to be in good agreement with a LCAO prediction of reconstruction of $n(\boldsymbol{p})$ [12]. A similar reconstruction has been made with the GaAs data reported here.

Recently attention has turned from pure to compound semiconductors. Pseudopotential calculations for compound semiconductors [15] indicate a decrease in the Compton profile anisotropy from elemental through III–V and II–VI semiconductors which is consistent with the increasing ionic trend in bonding character. Directional Compton profile of the compound semiconductor GaP have been deduced using ^{241}Am 59.5 keV γ-radiation [16]. However, the unavailability of a suitable theoretical model prevented quantitative interpretation of the results. The present study represents a comprehensive experimental study of the momentum density in GaAs and a detailed comparison with pseudopotential theory.

2. Measurements and data analysis

Five directional Compton profiles along the [100], [110], [111], [112] and [221] crystallographic axes of GaAs were deduced from measurements on the ^{198}Au Compton spectrometer [17] which is sited at the Rutherford–Appleton Laboratory. The lower energy, lower resolution measurements were made at the University of Warwick using the ^{241}Am spectrometer [18]. In the high energy measurements, each spectrum was accumulated over a period of 2–5 d depending upon the source activity (initially 150–200 Ci: the ^{198}Au isotope has a half-life of 2.7 d). Fifteen days were required for the low energy measurements with the 5 Ci ^{241}Am isotope which has a half-life of 452 years. Integrated counts of 6.4×10^6 (7.5×10^5 for [112] and [221] profiles) and

10^6 counts were accumulated in the respective high- and low-energy Compton profiles. The single-crystal samples used for this study were cut and shaped into discs of diameter 15.00±0.05mm and average thickness 1.82±0.02mm.

The data were processed by application of a series of energy dependent corrections applied according to a well tested scheme detailed elsewhere [19]. Particular attention was paid to the following corrections: the detector response function, the variation of detector efficiency with energy, the source-dependent and independent background corrections and multiple scattering within the source and sample.

The scattering angle of the ^{198}Au spectrometer was chosen to be 167° which defines the Compton peak energy to be 158.94 keV. A weak ^{123m}Te γ-source (E_γ = 159.00 keV) can then be used to measure the detector response function at the Compton peak energy. In this resolution measurement the sample–detector geometry of the scattering experiment was carefully mimicked to ensure that an appropriate measurement of the detector response function was obtained. In the lower energy experiment the detector response of the ^{241}Am spectrometer cannot easily be measured at the Compton peak energy (48.6 keV) and, as usual, a 60 keV response function was taken to represent the 48 keV response convolved with geometrical and source broadening effects [20]. An accurate estimation of the energy dependence of the ^{198}Au detector efficiency was derived from the prediction of a Monte Carlo simulation of the detector efficiency together with the efficiency measurements of the spectrum of a ^{133}Ba radioisotope which has several lines of known intensity in the energy range 50–400 keV. The ^{241}Am data did not have to be corrected for detector efficiency: it is essentially constant and close to 100% over the profile region.

The measured energy spectrum, $M(\omega)$ in a typical Compton experiment contains a background, $B(\omega)$ which must be removed before the remaining data reduction procedures can be implemented. This background comprises three main contributions, firstly, scattering of the primary radiation from the sample holder and/or the walls of the spectrometer chamber, secondly, radiation directly from the source and thirdly, cosmic rays and radiation from adjacent laboratories.

The magnitudes of the first two contributions are dependent upon the source activity and together form the 'dynamic background' component, whereas the third contribution is independent of the source activity and will be termed the 'static background'. Measurements performed using this 60 keV spectrometer are not susceptible to the effects of source decay due to the long half life of ^{241}Am (452 years) and the static background contribution is eliminated by a simple subtraction. Measurements performed using the ^{198}Au spectrometer require the subtraction of a static background from both $M(\omega)$ and $B(\omega)$ before correcting for source decay. The static background contribution was determined from an independent measurement with the source removed. In this study it was found to be approximately 40% of the total background at the Compton peak channel where the ratio of the Compton-to-background signals was 50:1.

A Monte Carlo simulation of the scattering [21] was employed to evaluate the multiple scattering contribution to the ^{198}Au data. It was assumed that the multiple profile had no directional dependence and the constant sample thickness ensured the same correction was applicable to each directional profile.

In the ^{241}Am experiment the breakdown of the impulse approximation for the Ga and As k-shell electrons (E_B=10.37 and 11.59 keV respectively) together with the difficulties encountered in removing systematic errors from $J(p_z)$ (see [19, 20, 4]) significantly reduce the reliability of the absolute profiles and hence these data were

only used for confirming the directional differences measured in the ^{198}Au experiment. Because the multiple scattering component is isotropic the ^{241}Am data were not corrected for multiple scattering.

After application of the data reduction procedures the ^{198}Au data were left–right averaged and then normalised to the free-atom value of 25.318 electrons over the momentum range $0 < p_z < 7$ au. The resulting profiles were all found to reduce to the free-atom value at high momentum, i.e. $p_z > 3.0$ au. The profile symmetry is a severe test of the accuracy of the data reduction procedures. These profiles were found to exhibit a profile asymmetry (i.e. $[J(+p_z) - J(-p_z)]/J(0)$) which was less than 0.75% over the range $|p_z| < 10$ au and were reproducible to within $\pm 0.23\% J(0)$. Similarly the ^{241}Am data were normalised to a free-atom value of 24.861 electrons, a value which accounts for the K-shell binding edges of Ga and As.

3. Discussion of results

The experimental results reported here have been compared with a pseudopotential band structure calculation of the directional Compton profiles of GaAs [15]. In this calculation the momentum density was written in terms of the pseudovalence wavefunctions and then Fourier inverted to obtain the B-function $B(\boldsymbol{r})$. After calculating $B(\boldsymbol{r})$ for various $\boldsymbol{r}$, the corresponding directional Compton profiles were obtained for an arbitrary fine mesh of p_z by Fourier transforming the directional B-functions numerically according to equation (4).

3.1. Difference profiles

The experimental difference profiles derived from measurements with 60 keV and 412 keV γ-radiation are shown in figure 1. The pseudopotential profile anisotropies have been convolved with Gaussians of the appropriate widths and included as the full curves in figure 1. The experimental profiles are identical beyond $|p_z| = 2$ au and have been normalised to the free-atom area out to this momentum. The two independent sets of data obtained from the ^{198}Au and ^{241}Am spectrometers are in excellent mutual agreement. The ^{241}Am anisotropies are of slightly poorer statistical quality, typically $\pm 0.27\% J(0)$, than the ^{198}Au anisotropies, $\pm 0.23\% J(0)$, and the additional resolution broadening of the ^{241}Am spectrometer, i.e. 0.57 au compared with 0.4 au, is evident as a damping on the scale of the anisotropies.

The pseudopotential theory is in excellent agreement with all the experimental anisotropies, correctly predicting both the scale and oscillation frequency of the anisotropies. This is in contrast to a recent pseudopotential calculation for the Compton profiles of Si and Ge where the scale of the anisotropy was correctly predicted but the oscillation frequency was somewhat shorter than that observed experimentally [15].

The arrows in figure 1 indicate the positions of the (111) reciprocal lattice vector. The theory predicts a build up of momentum density at these values of p_z i.e. 0.51 au, 1.02 au, etc. and this is also observed experimentally. The Compton profile anisotropies of Ge have been reported elsewhere [10] with a momentum resolution of $\sim$0.45 au. After accounting for the superior resolution of the high energy GaAs data (0.4 au), the amplitudes of the Ge anisotropies were estimated to be 10–15% larger than the corresponding GaAs results. Furthermore, the Compton profile anisotropies in Ge extend to higher momentum values. The decrease in the scale of the anisotropy

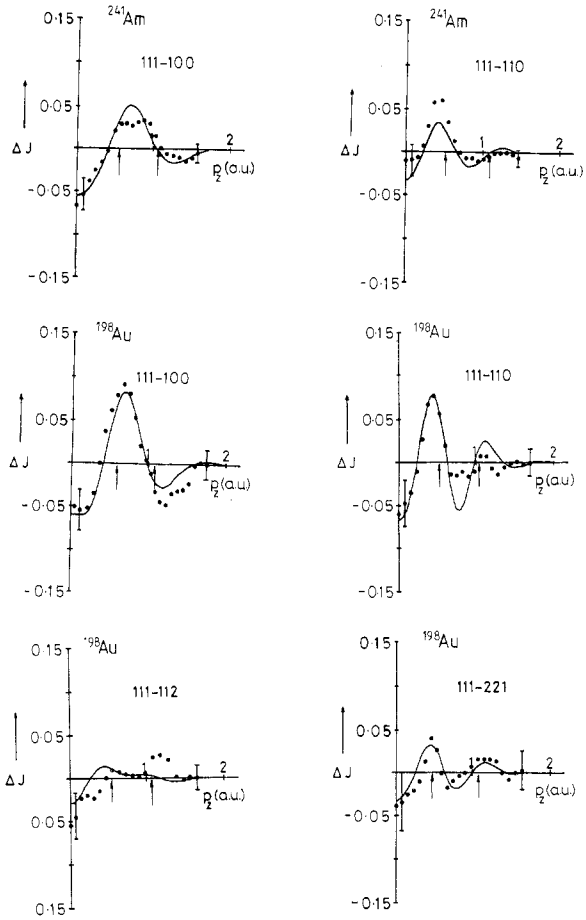

Figure 1. The experimental directional difference profiles of GaAs derived from Compton profile measurements with 60 keV and 412 keV γ-radiation. The predictions of the pseudopotential theory (full curves) have been convolved with a Gaussian of the appropriate FWHM (0.4 au for ^{198}Au, 0.57 au for ^{241}Am). The positions of (111) planes in the GaAs reciprocal lattice are indicated by the arrows. Both experiment and theory predict a build up of momentum density at these values of p_z, i.e. at 0.51 au, 1.02 au, etc.

according to the serial order of elemental and group III–V semiconductors has been attributed [15] to the increase in ionic bond character.

3.2. Absolute profiles

The absolute directional profiles of GaAs deduced from measurements with 412 keV γ-radiation are listed in table 1. The pseudopotential directional profiles and a composite Hartree Fock [22] free-atom profile of GaAs are also included. A free-atom core has been added to the pseudopotential profiles. All theories have been convolved with a Gaussian of FWHM=0.4 au which matches the experimental resolution.

Figure 2 shows the difference between the pseudopotential calculation and the [111] directional profile of GaAs measured with 412 keV γ-radiation. The form of this curve is characteristic of the other directional profiles which have been excluded

Table 1. Experimental and theoretical Compton profiles of GaAs measured along the [100], [110], [111], [112] and [221] crystallographic directions with 412 keV γ-radiation. The pseudopotential [15] and Hartree–Fock free-atom [22] theoretical Compton profiles have been convolved with a Gaussian of FWHM 0.4 au to mimic the experimental resolution.

	[100]		[110]		[111]		[112]		[221]		
p_z	Exp.	Pseudo.	Exp.	Pseudo.	Exp.	Pseudo.	Exp.	Pseudo.	Exp.	Pseudo.	Free-atom
0.0	12.038±0.020	12.750	12.118	12.742	11.995	12.734	12.155	12.794	12.086	12.814	13.486
0.1	11.987	12.734	12.044	12.798	11.939	12.678	12.070	12.720	12.022	12.722	13.316
0.2	11.867	12.591	11.840	12.625	11.755	12.487	11.866	12.495	11.826	12.489	12.831
0.3	11.498	12.282	11.505	12.124	11.468	12.192	11.586	12.168	11.529	12.174	12.098
0.4	11.062	11.809	11.064	11.577	11.083	11.767	11.189	11.735	11.102	11.699	11.217
0.5	10.496	11.109	10.538	10.947	10.561	11.165	10.641	11.147	10.561	11.075	10.296
0.6	9.832	10.233	9.952	10.295	9.924	10.393	9.994	10.389	9.970	10.383	9.427
0.7	9.132	9.313	9.297	9.690	9.237	9.461	9.305	9.465	9.292	9.543	8.668
0.8	8.481	8.220	8.596	8.561	8.549	8.284	8.614	8.290	8.588	8.353	8.044
0.9	7.882	7.526	7.958	7.491	7.907	7.534	7.973	7.527	7.942	7.530	7.548
1.0	7.376	7.154	7.428	6.971	7.378	7.127	7.420	7.108	7.397	7.089	7.161
1.2	6.674	6.546	6.663	6.507	6.626	6.504	6.656	6.514	6.638	6.503	6.606
1.4	6.208	6.076	6.215	6.087	6.181	6.066	6.236	6.070	6.211	6.071	6.170
1.6	5.835	5.723	5.858	5.733	5.831	5.731	5.832	5.729	5.824	5.731	5.850
1.8	5.477	5.393	5.495	5.388	5.458	5.395	5.507	5.396	5.483	5.396	5.501
2.0	5.108±0.015	5.035	5.141	5.039	5.108	5.034	5.137	5.034	5.097	5.034	5.140
2.5	4.227		4.235		4.215		4.249		4.254		4.248
3.0	3.409		3.419		3.437		3.436		3.426		3.429
4.0	2.248±0.011		2.229		2.234		2.220		2.264		2.227
5.0	1.563		1.537		1.567		1.531		1.533		1.522
6.0	1.174		1.139		1.175		1.124		1.165		1.109
7.0	0.898		0.861		0.903		0.854		0.867		0.536

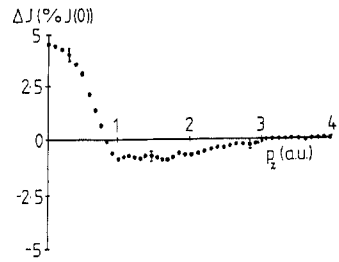

Figure 2. The difference between the experimental and theoretical [111] directional Compton profiles of GaAs. The experimental profile was derived from a measurement with 412 keV γ-radiation and the theoretical profile has been convolved with a Gaussian of FWHM 0.4 au. The theory is some 5% larger than the experimental result at low momentum and consequently smaller at high momentum. The disagreement arises because the pseudopotential model neglects the core orthogonalisation terms which are responsible for the high momentum components of the electron wavefunction.

from this figure for clarity. The calculated curve is some 5% larger than the experimental values at low momentum and is consequently smaller at high momentum. In the pseudopotential method the rapidly varying ion core potential is replaced by an effective potential which gives rise to the same electron wavefunctions outside the core as does the actual potential. However, this method neglects the core orthogonalisation terms [13] and therefore does not account for the large, local deviations in the valence wavefunctions which occur near the ion cores. These deviations give rise to the high-momentum components of the wavefunction, which in turn are responsible for the long tail of the Compton profile. It has been shown in [13] that although the effect of core orthogonalisation on the absolute Compton profile is large, it is approximately isotropic. Therefore systematic discrepancies in the absolute profiles will not affect the directional difference profiles.

3.3. B-functions

The reciprocal form factors of the [110] directional profile of GaAs obtained by Fourier transforming the ^{198}Au data and the pseudopotential calculation respectively are shown in figure 3. The theory has been convolved to match the experimental resolution of 0.4 au which in position space corresponds to a Gaussian damping function with FWHM=7.3 Å. At the origin the autocorrelation is complete and $B(0)$ is equivalent to the normalisation of the wavefunctions i.e. $B(0) = 64$ for GaAs. The statistical error in $B(z)$ is constant across the whole range of z and is given by $\sigma = B(0)/\sqrt{N_{\text{tot}}}$, where N_{tot} is the integrated area of the profile [5].

The [110] direction is illustrated because it exhibits the most prominent oscillations of all the five directions measured. The theory is in good agreement with the experiment, which indicates that the omission of the core orthogonalisation terms does not influence the B-function outside the core region over the spatial range shown. Both experiment and theory have zero passages at the first and second lattice translation distances (z = 3.98 Å and 7.96 Å, respectively) indicated by the arrows in figure 3 although the oscillations of the B-function are damped out at large z by the resolution of the experiment.

The largest interatomic separation in GaAs is found along the (100) crystallographic direction. The accumulation of charge will be a minimum for this interatomic

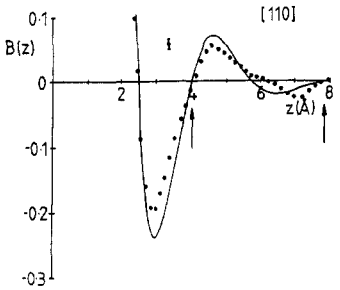

Figure 3. The reciprocal form factor $B(z)$ along the [110] direction in GaAs measured with 412 keV γ-radiation. The pseudopotential theory has been multiplied by an appropriate resolution factor before comparison with experiment. The arrows denote the first and second lattice translation distances i.e. $z = 3.98$ Å and 7.96 Å. The other zero passages are related to the particular form of the Bloch wavefunctions (see equation (6)). The statistical errors are independent of z.

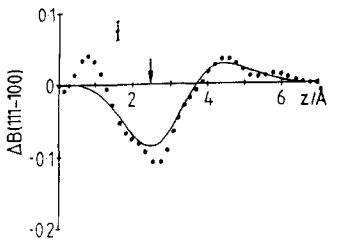

Figure 4. The theoretical and experimental difference $\Delta B(111 - 100)$ for GaAs. The theoretical curve has been damped by the appropriate resolution function. The arrow denotes the bond distance along the (111) nearest neighbour direction i.e. $\sqrt{3}a/4 = 2.44$ Å.

direction and a maximum for the nearest-neighbour direction i.e. the [111] direction. Therefore the difference $\Delta B([111] - [100])$ should reveal the strongest effects of bond anisotropy. From figure 4 it is clear that the striking bond anisotropy for GaAs predicted by the theory can also be observed experimentally. The arrow denotes the nearest neighbour bond distance (i.e. $\sqrt{3}a/4 = 2.44$ Å). The positive feature in the experimental data at ~0.8 au is not produced by the theory and was also absent from both the observed and calculated $\Delta B(111 - 100)$ anisotropy of diamond [23]. This feature is $\sim 4\sigma$ in magnitude and was also observed in the low energy data, however at present, its origin is not understood.

3.4. 3D electron momentum density

The 3D electron momentum density, $n(\boldsymbol{p})$ has been reconstructed using the double Fourier inversion technique [14]. This method involves the expansion of the B-function in terms of the spherical harmonic functions $Y_{l,m}(\theta, \phi)$, as follows

$$B(\boldsymbol{r}) = \sum_{l,m} b_{l,m}(\boldsymbol{r}) Y_{l,m}(\theta, \phi). \tag{7}$$

Both $B(\boldsymbol{r})$ and $n(\boldsymbol{p})$ have the Laue symmetry of the crystal which restricts the terms needed in the expansion. From measurements of a limited number of $B(z)$ it is possible

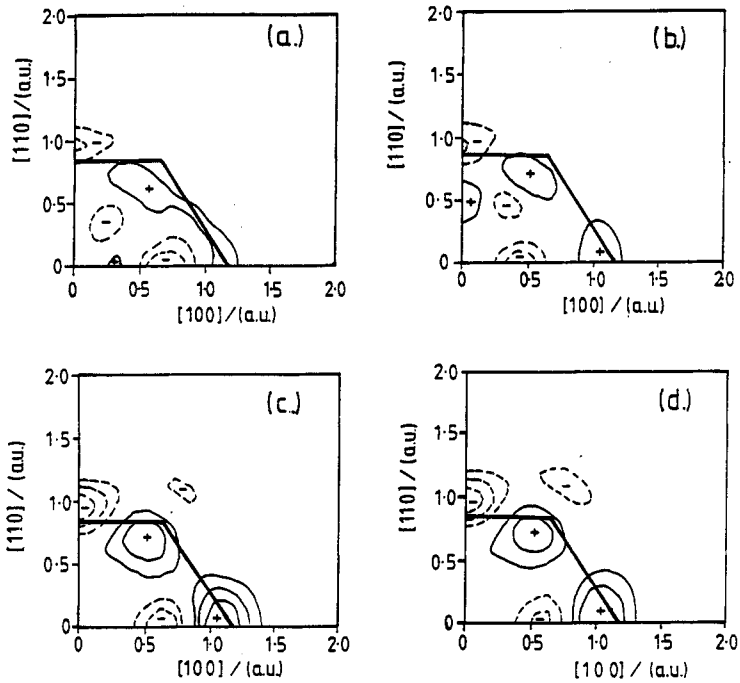

Figure 5. Experimental reconstructed anisotropy of the electron momentum density in GaAs using (*a*) five directional $B(z)$ and (*b*) three directional $B(z)$ functions. The total density is four valence electrons and the contours are 0.1 electron au^{-3}. The bold full line denotes the Jones zones. Shown in (*c*) and (*d*) is the theoretical reconstructed anisotropy of the electron momentum density in GaAs by the same procedure as (*a*) and (*b*) but based upon a pseudopotential band structure calculation [15] of the directional Compton profiles. The theoretical Compton profiles were convolved with the Gaussian experimental width of 0.4 au.

to determine the coefficients, $b_{l,m}$ in equation (7). The momentum density may be obtained from the Fourier transform of $B(\boldsymbol{r})$.

The reconstructed experimental anisotropy in the momentum density of GaAs is shown in figure 5(*a*). This was obtained using B-functions measured along five crystallographic axes, namely [100], [110], [111], [112] and [221], and four kinds of $Y_{l,m}(\theta,\phi)$ functions up to eighth order. The convergence of $n(\boldsymbol{p})$ was checked by altering the number of B-functions used in the reconstruction. Using three B-functions along the [100], [110] and [111] and three kinds of $Y_{l,m}(\theta,\phi)$ functions up to sixth order produced a similar momentum density anisotropy as illustrated in figure 5(*b*). The momentum density anisotropy predicted by the pseudopotential model has been determined from the directional Compton profiles in the same manner and is shown in figures 5(*c*) and (*d*).

It is apparent from figure 5 that increasing the number of B-functions used in the reconstruction has little effect on either the experimental or theoretical momentum density anisotropies. This suggests that five independent directional measurements of $B(z)$ are sufficient to reconstruct the 3D momentum density in the compound semiconductor GaAs.

Good agreement is observed between experiment and theory, which is in line with the good agreement observed between the experimental and theoretical Compton pro-

file anisotropies. In both the experimental and theoretical reconstructions a positive electron density exists along the [111] direction, which is compensated by a negative electron density along the [100] and [110] directions, but only inside the Jones zones. This feature reflects the bonding nature in tetrahedrally bonded semiconductors however the amplitudes of the momentum density anisotropy is smaller than that found in Si [14, 24] or Ge [13]. This enforces the prediction that the covalency decreases while the degree of ionicity increases according to the serial order of elemental and III–V semiconductors.

4. Summary

Careful revision of the data processing procedures has enabled very accurate directional Compton profiles to be measured for GaAs. The absolute experimental profiles exhibit good profile symmetry and are free from base line errors within the statistical accuracy of the data.

It is apparent from this study that the pseudopotential approach is well suited to describing the momentum anisotropy and the real space behaviour of the valence electron density of GaAs outside the core. The predicted decrease in the scale of the anisotropy in going from Ge to GaAs appears to be consistent with the increase in ionicity of the bond. In addition the striking bond anisotropy predicted for GaAs by the theory can also be observed experimentally. However, the theory is unsuccessful in describing the total electron density distribution due to the omission of the core orthogonalisation terms from the pseudo valence electron wavefunctions.

Acknowledgments

We wish to express our gratitude to the Japanese Society for the Promotion of Science (MJC) and to the British Council (DNT) for financing the exchange visit between Sendai and Warwick. The experimental work forms part of a programme of research work supported by the SERC in the United Kingdom.

References

[1] Williams B G (ed) 1977 *Compton Scattering* (New York: McGraw-Hill)
[2] Cooper M J 1985 *Rep. Prog. Phys.* **48** 415
[3] Bauer G E W and Schneider J R 1985 *Phys. Rev.* B **31** 681
[4] Cardwell D A, Cooper M J and Wakoh S 1989 *J. Phys.: Condens. Matter* **1** 541
[5] Pattison P and Schneider J R 1978 *Solid State Commun.* **28** 581
[6] Schulke W 1977 *Phys. Status Solidi* b **82** 229
[7] Pattison P and Weyrich W 1979 *J. Phys. Chem. Solids* **40** 213
[8] Lock D G, Crisp V H C and West R N 1973 *J. Phys. F: Met. Phys.* **3** 561
[9] Mijnarends P E 1979 *Positrons in Solids* ed P Hautojärvi (Berlin: Springer) pp 25–88
[10] Reed W A and Eisenberger P 1972 *Phys. Rev.* B **6** 4596
[11] Wepfer G G, Euwema R N, Surrat G T and Wilhite D L 1974 *Phys. Rev.* B **9** 2670
[12] Seth A and Ellis D E 1977 *J. Phys. C: Solid State Phys.* **10** 181
[13] Nara H, Shindo K and Kobayasi T 1979 *J. Phys. Soc. Japan* **46** 77
[14] Hansen N K, Pattison P and Schneider J R 1987 *Z. Phys.* B **66** 305
[15] Nara H, Kobayasi T and Shindo K 1984 *J. Phys. C: Solid State Phys.* **17** 3967

[16] Nageswar Rao M, Mohapatra D P, Panda B K and Pahdi H C 1985 *Solid State Commun.* **55** 241
[17] Holt R S, Cooper M J, DuBard J L, Forsyth J B, Jones T J L and Knight K M 1979 *J. Phys. F: Met. Phys.* **12** 1148
[18] Cooper M J, Holt R S and Dubard J L 1978 *J. Phys. E: Sci. Instrum.* **11** 1145
[19] Timms D N 1989 *PhD Thesis* University of Warwick
[20] Cardwell D A and Cooper M J 1986 *Phil. Mag.* B **54** 37
[21] Felsteiner J, Pattison P and Cooper M J 1974 *Phil. Mag.* **30** 537
[22] Biggs F, Mendelsohn L B and Mann J B 1975 *At. Data Nucl. Data Tables* **16** 201
[23] Pattison P, Hansen N K and Schneider J R 1981 *Chem. Phys.* **59** 231
[24] Mueller F M 1977 *Phys. Rev.* B **15** 3039